Journal of Solid State Chemistry 181 (2008) 2976–2982

Contents lists available at ScienceDirect

Journal of Solid State Chemistry

journal homepage: www.elsevier.com/locate/jssc

Crystal structure of $La_{0.4}Sr_{0.6}CoO_{2.71}$ investigated by TEM and XRD

C. Gspan [a,b,*], W. Grogger [a,b], B. Bitschnau [c], E. Bucher [d], W. Sitte [d], F. Hofer [a,b]

[a] Institute for Electron Microscopy and Fine Structure Research, Graz University of Technology, Steyrergasse 17, A-8010 Graz, Austria
[b] Centre for Electron Microscopy Graz, Steyrergasse 17, A-8010 Graz, Austria
[c] Institute of Physical and Theoretical Chemistry, Graz University of Technology, Technikerstrasse 4, A-8010 Graz, Austria
[d] Department of General, Analytical and Physical Chemistry, University of Leoben, Franz-Josef-Strasse 18, A-8700 Leoben, Austria

ARTICLE INFO

Article history:
Received 24 January 2008
Received in revised form
26 June 2008
Accepted 29 June 2008
Available online 15 July 2008

Keywords:
Perovskite superstructure
TEM
Electron diffraction
XRD

ABSTRACT

The structure of the oxygen-deficient perovskite $La_{0.4}Sr_{0.6}CoO_{3-\delta}$ ($\delta = 0.29$) was investigated by transmission electron microscopy (TEM) and X-ray powder diffraction (XRD). Domains between 50 and 250 nm in size were observed in the electron microscope. Weak superstructure reflections were found with both X-ray and electron diffraction. Investigations of these superstructure reflections by selected area electron diffraction (SAED) and convergent beam electron diffraction (CBED) showed that the domains in a crystal are orientated in a 90° relationship. High-resolution transmission electron microscopy (HRTEM) images from the domain boundary also revealed a 90° orientation dependency. Using the symmetry of CBED patterns, the point group 4/*mmm* was determined. By comparing reflections from the SAED pattern with possible reflections, the space group *I*4/*mmm* (No. 139) could be isolated and finally the crystal structure was refined by Rietveld refinement.

1. Introduction

Oxygen vacancies in bulk materials and at internal interfaces in materials are responsible for many interesting mechanical, magnetic and electronic properties. In this respect, perovskite oxides are an important group of oxygen-deficient materials with several potential technological advantages. Especially, strontium–cobalt based perovskites exhibit a high ionic conductivity in addition to a high electronic conductivity [1], and as such possess significant potential for solid oxide fuel cells, oxygen transport membranes and gas sensors.

Recently, we found that the ionic conductivity of $La_{0.4}Sr_{0.6}CoO_{3-\delta}$ (LSCO) exhibits a temperature-dependent maximum as a function of the oxygen non-stoichiometry [1,2]. This effect indicates the possible onset of vacancy ordering with decreasing oxygen content and temperature. In order to study this phenomenon in the transmission electron microscope (TEM), a sample with well-defined oxygen deficiency was prepared. $La_{0.4}Sr_{0.6}CoO_{3-\delta}$ was annealed at $p(O_2) = 1 \times 10^{-3}$ bar at 825 °C for 60 h and subsequently rapidly quenched to room temperature. This way the oxygen deficiency was "frozen in" to obtain the material with $\delta = 0.29$ at room temperature. TEM investigations revealed a superstructure and domains in these samples [3]. However, it was not possible to find a full crystallographic explanation of these particular morphological features.

The crystallography of La–Sr–Co-oxides has been investigated in several studies, some also reporting superstuctures. For example, X-ray powder diffraction (XRD) results by Ohbayashi et al. [4] revealed a rhombohedral structure for the oxygen stoichiometric $La_{1-x}Sr_xCoO_3$ (synthesized by a ceramic technique) with low Sr contents and a cubic structure at $x = 0.6$ and higher. Similarly, for the stoichiometric sample $La_{1-x}Sr_xCoO_3$ (synthesized by solid phase reaction), Mineshige et al. [5] found a rhombohedral system with the space group *R*3-*c* in the range of $0.0 \leqslant x \leqslant 0.5$. With increasing Sr concentration, the rhombohedral distortion decreases and therefore in the range of $0.55 \leqslant x \leqslant 0.7$ a cubic structure with the space group *Pm*3*m* was found. Ravindran et al. [6] reported a cubic phase for $La_{1-x}Sr_xCoO_3$ with x values greater than 0.5. Wang and Zhang [7] investigated thin films of $La_{1-x}Sr_xCoO_3$ grown by liquid source metal–organic chemical-vapour deposition (MOCVD) on $LaAlO_3$ and found microdomains (30–200 nm) with a tetragonal structure but without information about the corresponding space group. Extensive studies on the structure of rare earth cobaltates $Ln_{1-x}Sr_xCoO_{3-\delta}$ ($Ln = La^{3+}$, Pr^{3+}, Nd^{3+}, etc.) with various Sr contents were summarized in phase diagrams by James et al. [8] who also reported that $La_{1-x}Sr_xCoO_{3-\delta}$ with $x = 0.6$ has a cubic structure.

According to van Doorn and Burggraaf [9], the XRD pattern of $La_{0.4}Sr_{0.6}CoO_{3-\delta}$ shows a cubic symmetry. Additional low intensity reflections were only observed for $La_{0.3}Sr_{0.7}CoO_{3-\delta}$ suggesting a superstructure on the basis of doubling one unit cell axis. While

* Corresponding author at: Institute for Electron Microscopy and Fine Structure Research, Graz University of Technology, Steyrergasse 17, A-8010 Graz, Austria. Fax: +43 316 811 596.
E-mail address: christian.gspan@felmi-zfe.at (C. Gspan).

0022-4596/$ - see front matter © 2008 Elsevier Inc. All rights reserved.
doi:10.1016/j.jssc.2008.06.058

these reflections were not found in a supplementary neutron powder diffraction study, high-resolution transmission electron microscopy (HRTEM) and SAED studies of $La_{0.3}Sr_{0.7}CoO_{3-\delta}$ showed microdomains in the range of 5–50 nm with superstructure reflections. About 40% of the sample volume exhibited superstructure reflections in the electron diffraction pattern. For this phase, van Doorn and Burggraaf proposed a tetragonal superstructure cell originating from the ordering of oxygen vacancies.

Among various rare earth cobaltates $Ln_{1-x}Sr_xCoO_{3-\delta}$ (Ln = La, Pr and Nd) two oxygen-deficient perovskite phases $La_{0.33}Sr_{0.67}CoO_{3-\delta}$ ($\delta = 0.21$) and $La_{0.10}Sr_{0.90}CoO_{3-\delta}$ ($\delta = 0.19$) (synthesized by sol–gel chemistry) were investigated by James et al. [10]. With X-ray diffraction, no superstructure was observed and the crystal system could be indexed as cubic. However, in the electron and neutron diffraction patterns, additional weak superstructure reflections were observed and the system was determined as tetragonal ($P4/mmm$).

While various studies on the structure of $La_{1-x}Sr_xCoO_{3-\delta}$ can be found in the literature [4–10] the samples differ with respect to synthesis route, La/Sr ratio and oxygen content. Frequently, the oxygen non-stoichiometry is not further specified or $\delta = 0$ is assumed. However, previous studies showed that depending on the thermal pre-treatment and the $p(O_2)$ up to 10% of the oxygen sites can be vacant [1]. Consequently, the present study concentrates on a careful investigation of the non-stoichiometric sample $La_{0.4}Sr_{0.6}CoO_{2.71}$ with well-defined oxygen deficiency in order to understand the superstructure, the domains, and the relationship between both from a crystallographic point of view.

2. Experimental

2.1. Synthesis

For the synthesis of the sample, the glycine nitrate process was applied. Adequate ratios of 1 M cation nitrate solutions were mixed with glycine as a chelating and combustion agent to obtain the composition $La_{0.4}Sr_{0.6}CoO_{3-\delta}$ [11]. By heating on a hot plate water was evaporated to form a gel which self-ignites. The raw ash was fired for 4 h at 1000 °C in air. The resulting powder was ball-milled, pressed into tablets and sintered in air for 4 h at 1400 °C. The tablets were annealed at $p(O_2) = 1 \times 10^{-3}$ bar at 825 °C for 60 h and subsequently quenched to room temperature to obtain $La_{0.4}Sr_{0.6}CoO_{2.71}$ with a defined oxygen non-stoichiometry $\delta = 0.29$ [1] which was determined by thermogravimetry. The chemical composition of the crystal was individually checked by energy-dispersive X-ray spectrometry (EDXS) in the TEM (Tracor-Noran with HPGe detector).

2.2. Transmission electron microscopy (TEM)

Bright field images and electron diffraction patterns were acquired using a Philips CM20 TEM (with a LaB_6 cathode) and a Tecnai F20 (schottky gun), both operating at 200 kV. Energy filtered diffraction patterns were acquired on the TF20 with a post column energy filter (Gatan Imaging Filter, GIF) and were zero-loss filtered (i.e. elastically scattered electrons only). For the microscopic investigations, the samples were prepared by dispersing finely ground material onto a holey carbon film. In order to take care of the radiation sensitive nature of the investigated materials, special attention was paid to changes in the crystallographic structure of the specimens. Thus, HR-TEM images and/or electron diffraction patterns were made before and after each acquisition (in particular HR-TEM images and CBED patterns) to make sure that no changes due to the electron irradiation had happened.

2.3. Powder X-ray diffraction (XRD)

X-ray powder diffraction measurements were made on a Philips Expert diffractometer with Bragg Brentano Geometry using Cu$K\alpha$ radiation. Data were collected with steps of 0.02° and with 35 s per step in the region 10–70° (2θ). Rietveld refinements [12] were carried out with the programs X-Pert Plus [13] and Fullprof [14].

3. Results and discussion

3.1. Powder X-ray diffraction (XRD) and transmission electron microscopy (TEM)

In a first try, the X-ray diffraction spectrum for $La_{0.4}Sr_{0.6}CoO_{2.71}$ over the 2θ range from 10° to 75° was indexed cubic ($a = b = c = 0.7705$ nm) as shown in Fig. 1. However, at $2\theta = 11.4°$, an additional low intensity peak was found (Fig. 1) and interpreted as a superstructure reflection. Ohbayashi et al. [4] found a similar X-ray diffraction pattern for stoichiometric $La_{1-x}Sr_xCoO_3$, but without a superstructure peak at 11.4°. The structure of this material was described as a cubic distorted perovskite.

As already described previously [1,2], TEM bright field images of most of the $La_{0.4}Sr_{0.6}CoO_{2.71}$ grains show a typical domain structure, i.e. bright and dark regions (Fig. 2b and c) with a width of about 50–250 nm and a length of up to 1 μm. However, these domains could not be observed for particles smaller than 100 nm. This typical morphology has not been reported for other La–Sr–Co-oxides. Dependent on the orientation of the investigated crystal, the domains may look very differently. If the domains are in the main zone axes [1 0 0] or [0 0 1], they will not (or the boundaries between them) exhibit visible contrast in TEM bright field images (Fig. 2a). By tilting the sample a few degrees out of the main zone axis the domains become visible (Fig. 2b). The contrast of the domains may change significantly (compare Fig. 2b with c) by further tilting.

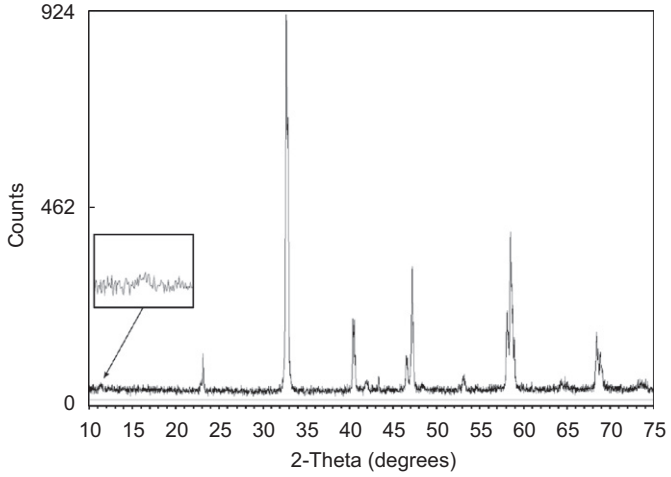

Fig. 1. X-ray diffraction profile of $La_{0.4}Sr_{0.6}CoO_{2.71}$ (arrow shows superstructure reflection at 11.4°).

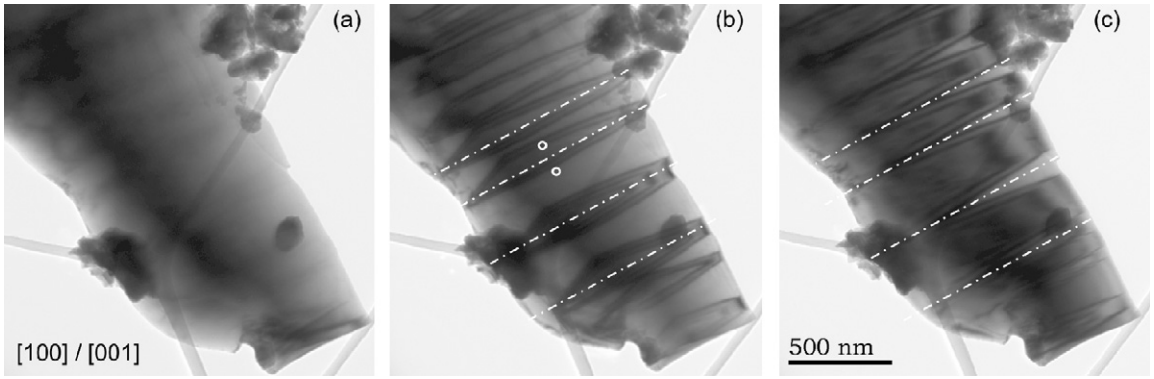

Fig. 2. TEM bright field images show domains, which change their appearance when tilting the specimen. Tilt angle from (a) to (b) about 2° and from (b) to (c) about 3°. In the main zone axes [1 0 0/0 0 1] (a) the domains are not visible. By slightly tilting out of the zone axis (b) the domains become visible (dotted lines) and the contrast of the domains further changes by tilting to (c).

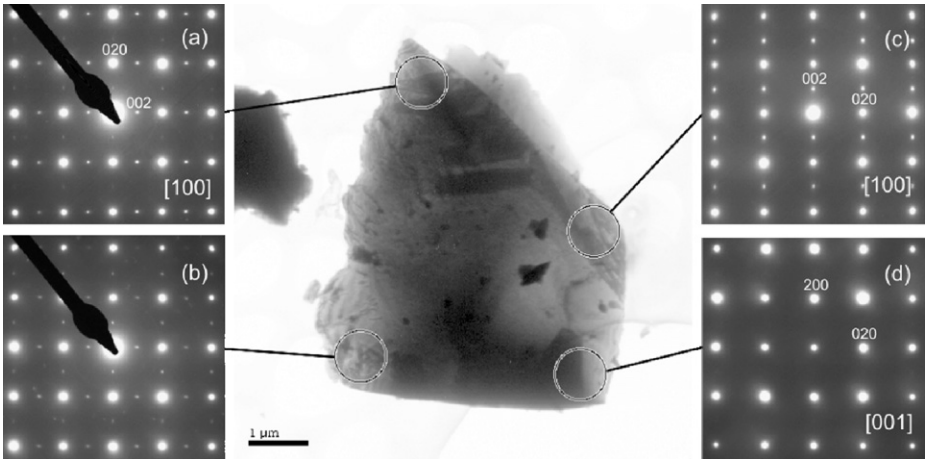

Fig. 3. $La_{0.4}Sr_{0.6}CoO_{2.71}$ crystal with corresponding ED patterns. (a) and (c) show in the [1 0 0] axis superstructure reflections (0 0 2) along one axis; (b) shows superstructure along two axes (two domains mutually rotated by 90°). In [0 0 1] there is no superstructure (d).

3.2. Selected area electron diffraction (SAED)

In our previous study of $La_{0.4}Sr_{0.6}CoO_{2.71}$ [2], electron diffraction was used to reveal a superstructure along a main zone axis orientation which mostly corresponded to the domain structure observed in the TEM images (see Fig. 2). A particular crystal was found in the present study which revealed four regions with different electron diffraction patterns in a main zone axis orientation (Fig. 3a–d). The diffraction pattern in Fig. 3a showed superstructure reflections (0 0 2) along one axis, while the pattern in Fig. 3c showed superstructure reflections (0 0 2) along the perpendicular direction. Both patterns are from zone axis [1 0 0]. The electron diffraction pattern from region b (Fig. 3b) had superstructure reflections along both axes (as we will later see this is the combination of at least two domains which are mutually rotated by 90°). Yet another region of this crystal showed a pattern (Fig. 3d) without superstructure in zone axis [0 0 1]. Earlier studies using X-ray, neutron and electron diffraction have already demonstrated that distinct microdomains with superstructures are present in $La_{0.3}Sr_{0.7}CoO_{3-\delta}$ as well as regions without such a superstructure [9].

3.3. High-resolution TEM

The HRTEM investigation of the boundary between two domains from the crystal shown in Fig. 3 showed two possible configurations. In the first type of domain boundaries both domains showed a superstructure rotated by 90° (Fig. 4a). The superstructure reflections (0 0 2) from the left domain can be seen in the Fast Fourier Transformation (FFT) in Fig. 4c. The FFT from the right domain in Fig. 4d shows the same superstructure reflections but with a 90° rotation compared to Fig. 4c. In another type, we found one domain with superstructure and the other one without superstructure (Fig. 4b). Consequently, the FFT from the right domain (Fig. 4f) shows no superstructure.

3.4. Convergent beam electron diffraction (CBED)

The investigation of the superstructure reflections originating from single domains by conventional electron diffraction (SAED) is limited by the smallest selected area aperture, which is in the range of 300 nm. In order to obtain superstructure reflections from single domains which are smaller than this limit, it is necessary to apply CBED [15].

CBED patterns were performed on areas corresponding to the circles in Fig. 2b. The patterns (Fig. 5) from these different positions were obtained under the same crystal orientation. The beam size was about 4 nm. The results were the same as for the HRTEM images, showing two possibilities for the superstructure of neighbouring domains. Either both domains show superstructure reflections or one domain shows no superstructure reflections (Fig. 5).

Convergent beam electron diffraction is also a useful method to obtain information about the crystallographic symmetry from

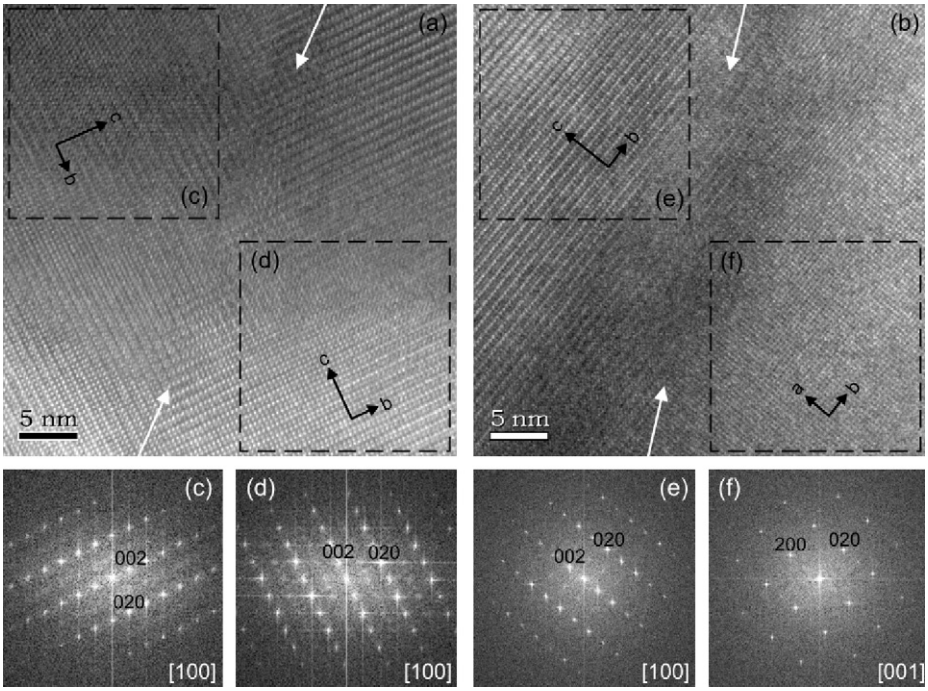

Fig. 4. HRTEM images from domain boundaries (white arrows) showing (a) superstructure on both sides of the boundary (c and d) and (b) superstructure only on the left side (e) and the right side without superstructure (f). Dashed windows indicate the areas of the corresponding FFTs below. (For comparing the FFTs from zone axis [1 0 0] with the electron diffraction patterns, see Fig. 8.)

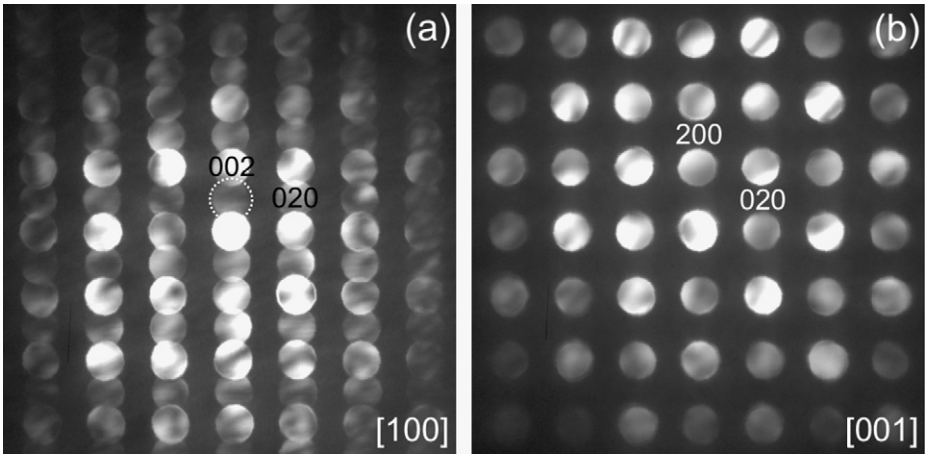

Fig. 5. CBED pattern from one domain shows superstructure reflections (0 0 2) (in circle) (a), whereas no superstructure reflections are observed in the neighbouring domain (b).

one single crystal. After Buxton et al. [16], the point group can be determined by using the symmetry from different kinds of CBED patterns. From the region d in Fig. 3, the bright field pattern (BP) (Fig. 6b) and also the whole pattern (WP) (Fig. 6a) have a four-fold rotation axis and two independent mirror planes, i.e. 4*mm* symmetry. The two dark-field patterns +DP and −DP (Fig. 6c and d) show in +G and −G a 2*mm* symmetry and coincide with the symmetry $21_R mm$. With this information, the diffraction group was determined to be $4mm1_R$. According to Buxton et al., the point groups 4/*mmm* and *m*3*m* are the only ones that correspond to the diffraction group $4mm1_R$. To distinguish between these two point groups, we had to analyse the electron diffraction pattern from the main zone axis [1 0 0] (Fig. 3c). This pattern is untypical for a cubic crystal system with the lattice parameters $a = b = c$. Therefore, it can be deduced that the crystal system is tetragonal and consequently the corresponding point group is 4/*mmm*. That the crystal system is tetragonal can also be seen in the electron diffraction pattern from zone axis [2 2 1] (Fig. 7). The symmetry of this pattern should be 3*m* for a cubic crystal system. However, this symmetry is broken in the first-order Laue zone (FOLZ) and the second-order Laue zone (SOLZ) as a result from the different lattice parameters ($a = b \neq c$). By moving the electron beam from one domain to the next, we can also investigate the change in the orientation of the c^*-axis, which is shorter than the a^*- and the b^*-axes in reciprocal space (compare Fig. 7a and b).

In the point group 4/*mmm* there are 20 possible space groups. By looking more closely at an electron diffraction pattern from the zone axis [1 0 0] additional weak reflections can be noticed (Fig. 8, $hkl = (0\,1\,1)$). These reflections are more clearly visible if the diffraction patterns are zero-loss filtered, removing the inelastically scattered electrons [17]. By using these weak reflections, the lattice type can be determined as body-centered. So the number of

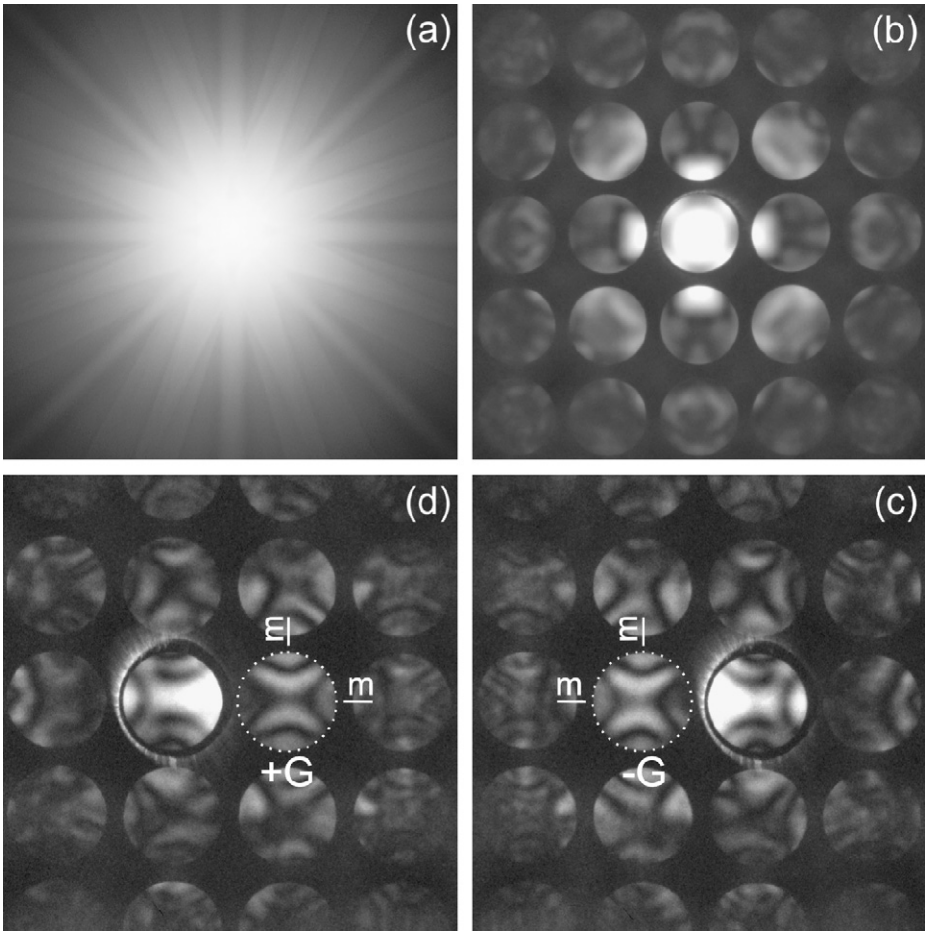

Fig. 6. Series of convergent beam electron diffraction patterns. Both the whole pattern (WP) (a) and the bright field pattern (BP) (b) show a 4*mm* symmetry. The dark field patterns (200 and −200 DP) show a 2*mm* symmetry (c and d).

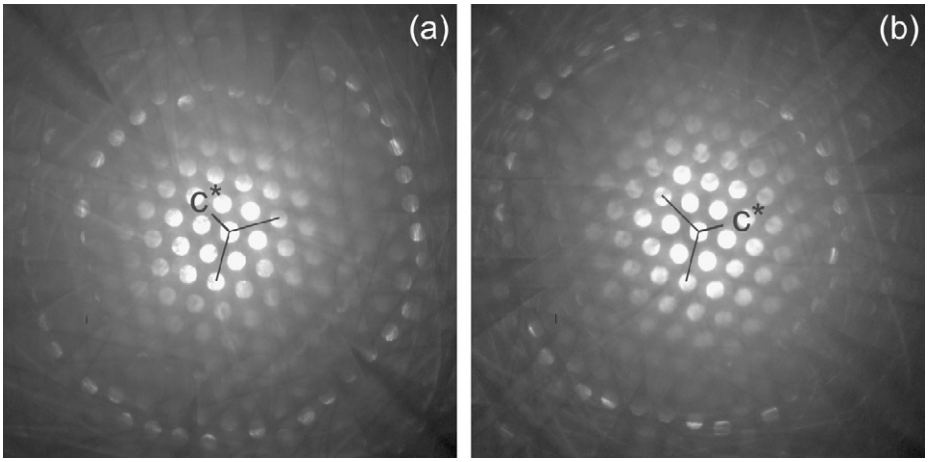

Fig. 7. CBED in zone axis [2 2 1] from two domains. The reduction of the symmetry from cubic 3*m* to *m* of a tetragonal crystal system allows the identification of the *c**-axis (a and b).

space groups can be reduced to four candidates (Nos. 139–142). In the XRD spectrum, we do not observe the (0 1 1) reflection, because the expected signal is weaker than the noise level. However, with electron diffraction, there is the possibility of a single crystal investigation and the peak was detected (Fig. 8). However, this (0 1 1) reflection is forbidden for the space group *I*4/*mcm* (No. 140) and for $I4_1/acd$ (No. 142). For the space group *I*4/*amd* (No. 141) the (0 1 1) reflection is allowed but the superstructure reflection (0 0 2) is forbidden. Only the space group *I*4/*mmm* (No. 139) offers the possibility for both detected reflections.

3.5. Structure model

Rietveld refinements were carried out for the space group *I*4/*mmm*. Final steps of the refinement included all atomic

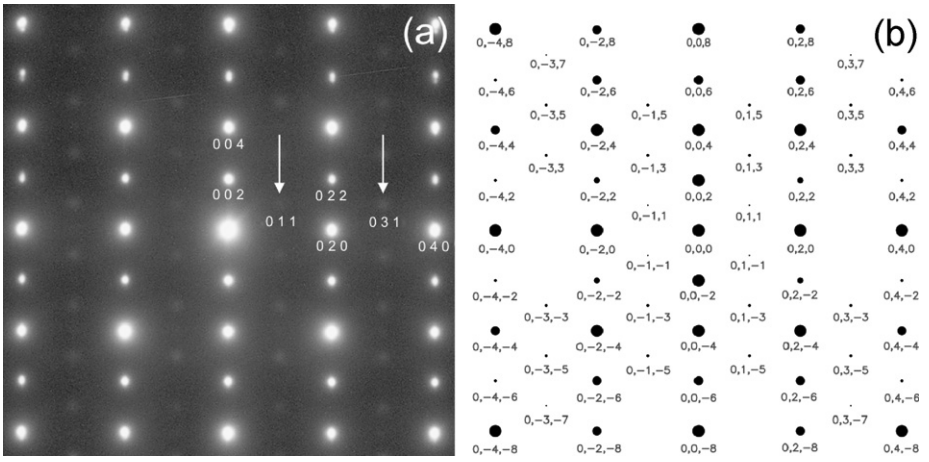

Fig. 8. (a) SAED in zone axis [1 0 0] with superstructure reflections and additional weak reflections (arrows). (b) Simulation for [1 0 0].

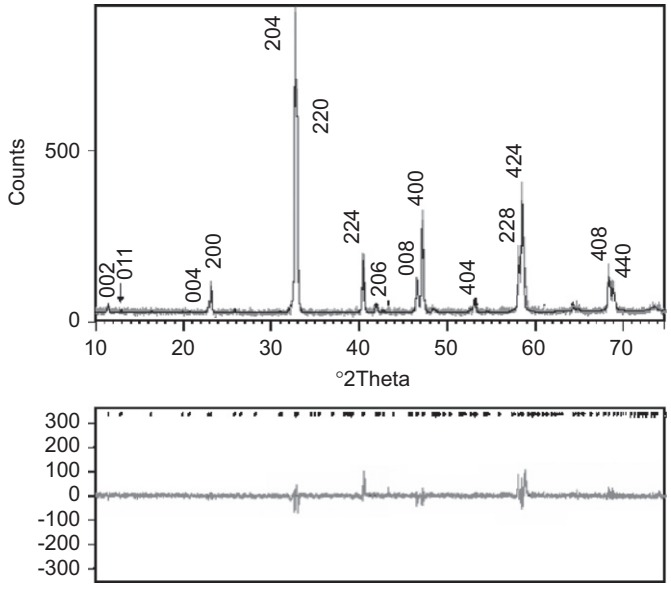

Fig. 9. XRD profile: observed data (grey), calculated profile (dark) and the difference plot below; tick marks represent the allowed reflections.

Table 1
Refined X-ray data for $La_{0.4}Sr_{0.6}CoO_{2.71}$ ($R_p = 16.1$, $R_{Bragg} = 7.04$), occupancy and atomic fractional coordinates

Atom	Wyck	s.o.f.	*x*	*y*	*z*
Sr1	4*e*	0.600000	0.000000	0.000000	0.865(2)
Sr2	8*g*	0.600000	0.000000	0.500000	0.871(1)
Sr3	4*e*	0.600000	0.000000	0.000000	0.364(2)
La1	4*e*	0.400000	0.000000	0.000000	0.865(2)
La2	8*g*	0.400000	0.000000	0.500000	0.871(1)
La3	4*e*	0.400000	0.000000	0.000000	0.364(2)
Co1	8*h*	1.000000	0.748(2)	0.748(2)	0.000000
Co2	8*f*	1.000000	0.250000	0.250000	0.250000
O1	16*n*	1.000000	0.000000	0.26(1)	0.234(3)
O2	16*m*	1.000000	0.285(3)	0.285(3)	0.112(2)
O3	8*i*	1.000000	0.000000	0.820(9)	0.000000
O4	8*j*	0.420000	0.15(5)	0.50000	0.000000

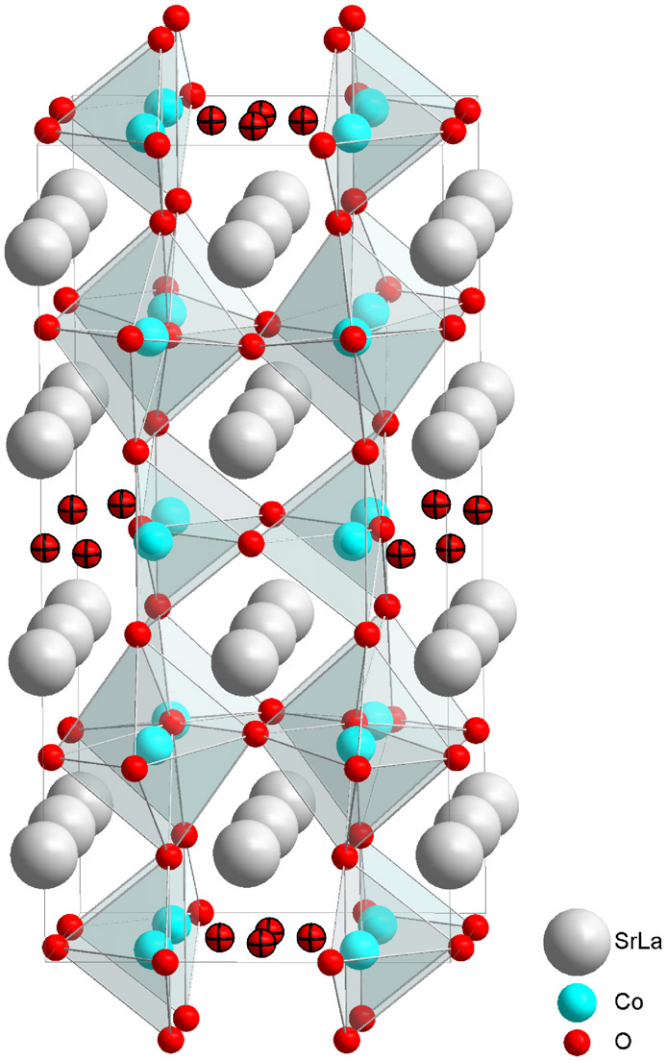

Fig. 10. The structure of $La_{0.4}Sr_{0.6}CoO_{2.71}$; vacant oxygen positions are indicated by black crosses.

coordinates (constrained). The background was modelled with a polynomial, the profile was fitted with a pseudo-Voigt function. A small preferred orientation along [0 0 1] was included in the refinement. The obtained lattice parameters are $a = b = 0.77111$ nm and $c = 1.5613$ nm. An example of the profile fit is shown in Fig. 9. The refined atomic positions and derived interatomic distances are summarized in Table 1. The structure model with the space group

*I*4/*mmm* (Fig. 10) is in good agreement with the experimental XRD-data.

Finally, the electron diffraction pattern from zone axis [1 0 0] was simulated [18] using the space group *I*4/*mmm* (Fig. 8b) which gives a good correlation with the experiment shown in Fig. 8a. Also the very weak reflection (0 1 1), which can be seen more clearly in zero-loss filtered patterns, correlates well with the simulation. This diffraction pattern is of the same type as the one shown by van Doorn and Burggraaf [9] for $La_{0.3}Sr_{0.7}CoO_{3-\delta}$ aligned along the main axis. However, the authors only showed electron diffraction patterns which are characteristic of an orientationally twinned tetragonal superstructure phase (such as in Fig. 3b), because they could not analyse a single domain region to obtain a single domain electron diffraction due to the small domain size (~10–30 nm) in their materials. This small domain size may also explain why the additional superstructure reflections are not visible in neither XRD nor neutron powder diffraction patterns. Additionally, the pattern by van Doorn et al. does not reproduce the weak (0 1 1) reflection.

In the present study, we find larger domains than in prior work which can be individually studied by electron diffraction methods such as CBED and even SAED (see Fig. 8a which is characteristic of a single domain region). The formation and growth of the domains were obviously enhanced by annealing the $La_{0.4}Sr_{0.6}CoO_{2.71}$ powder at 825 °C for 60 h.

The superstructure along the *c*-axis is characteristic for this non-stoichiometric $La_{0.4}Sr_{0.6}CoO_{2.71}$ sample (Fig. 10). This could be related to the localization of the randomly distributed oxygen vacancies at special oxygen positions (only O4, see Table 1). This can be described as oxygen vacancy ordering. The result agrees well with the proposed superstructure for $La_{0.3}Sr_{0.7}CoO_{3-\delta}$ by van Doorn and Burggraaf [9] where the missing oxygen anions are only present in every second (0 0 1) (La/Sr)O plane. For this model, van Doorn and Burggraaf [9] used a tetragonal system ($a_c \times a_c \times 2a_c$) without further information about point group, space group and atom positions. In their model, there is also no octahedron tilting and no localization of the oxygen vacancies at O4. The structure model also agrees with the work of James et al. [8], who also found the space group *I*4/*mmm* for $Y_{0.1}Sr_{0.9}Co_{3-\delta}$ and for all other perovskites $Ln_{0.1}Sr_{0.9}CoO_{3-\delta}$ with *Ln* from Sm to Yb.

These results disagree with some previous findings by other authors. Possible reasons could be differences in preparation methods, thermal pre-treatment, and/or the amount of oxygen vacancies (δ). It has been shown previously that the homogeneity of LSCO samples is strongly influenced by the preparation method [2]. In our investigation, we checked the chemical composition and homogeneity very carefully and the δ-value was determined accurately by thermogravimetry [19].

4. Conclusions

The crystal structure of the oxygen-deficient perovskite $La_{0.4}Sr_{0.6}CoO_{2.71}$ was studied by means of TEM, electron diffraction and powder X-ray diffraction. High-resolution TEM and CBED investigations disclosed twinned domains with 90° orientation. Additionally, convergent electron diffraction revealed the point group 4/*mmm* and the combination of XRD and ED showed a tetragonal superstructure with the space group *I*4/*mmm*. This result agrees with previous findings by van Doorn and Burggraaf [9] who proposed a tetragonal superstructure without giving a space group. Our study demonstrates that CBED may serve as a valuable tool in crystal structure investigations of submicron crystals in addition to conventional high-resolution TEM imaging.

Acknowledgments

The authors gratefully acknowledge the financial support by the *Austrian Science Funds* within the Special Research Program (SFB) *Electroactive Materials.*

References

[1] E. Bucher, W. Sitte, I. Rom, I. Papst, W. Grogger, F. Hofer, Solid State Ionics 152/153 (2002) 417.
[2] I. Rom, F. Hofer, E. Bucher, W. Sitte, K. Gatterer, H.P. Fritzer, A. Popitsch, Chem. Mater. 14 (2002) 135.
[3] I. Letofsky-Papst, W. Grogger, I. Rom, F. Hofer, E. Bucher, W. Sitte, Microsc. Microanal. 8 (Suppl. 2) (2002) 618.
[4] H. Ohbayashi, T. Kudo, T. Gejo, Jpn. J. Appl. Phys. 13 (1974) 1.
[5] A. Mineshige, M. Inaba, T. Yao, Z. Ogumi, K. Kikuchi, M. Kawase, J. Solid State Chem. 121 (1996) 423.
[6] P. Ravindran, P.A. Korzhavyi, H. Fjellvag, A. Kjekshus, Phys. Rev. B 60 (1999) 423.
[7] Z.L. Wang, J. Zhang, Phys. Rev. B 54 (1996) 1153.
[8] M. James, D. Cassidy, D.J. Goossens, R.L. Withers, J. Solid State Chem. 177 (2004) 1886.
[9] R.H.E. van Doorn, A.J. Burggraaf, Solid State Ionics 128 (2000) 65.
[10] M. James, T. Tedesco, D.J. Cassidy, R.L. Withers, Mater. Res. Bull. 40 (2005) 990.
[11] L.A. Chick, L.R. Pederson, G.D. Maupin, J.L. Bates, L.E. Thomas, G.J. Exarhos, Mater. Lett. 10 (1990) 6.
[12] H.M. Rietveld, J. Appl. Crystallogr. 2 (1969) 65.
[13] X'Pert Plus, Version 1.0, Program for Crystallography and Rietveld Analysis, Philips Analytical, 1999.
[14] J. Rodriguez-Carvajal, Physica B 192 (1993) 55.
[15] J.W. Steeds, Anal. Electron Microsc. Proc. Workshop (1981) 124.
[16] B.F. Buxton, J.A. Eades, J.W. Steeds, G.M. Rackham, Philos. Trans. R. Soc. Lond. 281 (1976) 171.
[17] D.B. Williams, J.W. Edington, Met. Sci. 9 (1976) 529.
[18] J.M. Zuo, J.C. Mabon, Web-based Electron Microscopy Application Software: Web-EMAPS, Microsc. Microanal. 10 (2004) 1000, 〈http://emaps.mrl.uiuc.edu/〉.
[19] E. Bucher, W. Jantscher, A. Benisek, W. Sitte, W. Preis, I. Rom, F. Hofer, Solid State Ionics 141/142 (2001) 375.